AGU PUBLICATIONS

JGR

Journal of Geophysical Research: Space Physics

RESEARCH ARTICLE
10.1002/2017JA024419

Key Points:
- Field configurations at high-latitude pre dusk magnetosphere are investigated at Saturn
- Swept forward field is found to be prevalent with an average angle of 23°
- Field is found to exhibit transient increases in sweep angle

Correspondence to:
E. H. Davies,
ewen.davies11@imperial.ac.uk

Citation:
Davies, E. H., Masters, A., Dougherty, M. K., Hansen, K. C., Coates, A. J., & Hunt, G. J. (2017). Swept forward magnetic field variability in high-latitude regions of Saturn's magnetosphere. *Journal of Geophysical Research: Space Physics*, *122*, 12,328–12,337. https://doi.org/10.1002/2017JA024419

Received 31 MAY 2017
Accepted 5 DEC 2017
Accepted article online 11 DEC 2017
Published online 26 DEC 2017

Swept Forward Magnetic Field Variability in High-Latitude Regions of Saturn's Magnetosphere

E. H. Davies[1], A. Masters[1], M. K. Dougherty[1], K. C. Hansen[2], A. J. Coates[3,4], and G. J. Hunt[1]

[1]The Blackett Laboratory, Imperial College London, London, UK, [2]Department of Atmospheric, Oceanic and Space Sciences, University of Michigan, Ann Arbor, MI, USA, [3]Mullard Space Science Laboratory, Department of Space and Climate Physics, University College London, Dorking, UK, [4]The Centre for Planetary Sciences, UCL/Birkbeck, London, UK

Abstract Swept forward field is the term given to configurations of magnetic field wherein the field lines deviate from the meridional planes of a planet in the direction of its rotation. Evidence is presented for swept-forward field configurations on Cassini orbits around Saturn from the first half of 2008. These orbits were selected on the basis of high inclination, spatial proximity, and temporal proximity, allowing for the observation of swept-forward field and resolution of dynamic effects using data from the Cassini magnetometer. Nine orbits are surveyed; all show evidence of swept-forward field, with typical sweep angle found to be 23°. Evidence is found for transient events that lead to temporary dramatic increases in sweep-forward angle. The Michigan Solar Wind Model is employed to investigate temporal correlation between the arrivals of solar wind shocks at Saturn with these transient events, with two shown to include instances corresponding with solar wind shock arrivals. Measurements of equatorial electron number density from anode 5 of the Cassini Plasma Spectrometer instrument are investigated for evidence of magnetospheric compression, corresponding with predicted shock arrivals. Potential mechanisms for the transfer of momentum from the solar wind to the magnetosphere are discussed.

1. Introduction

The Cassini spacecraft has been in orbit around Saturn since mid-2004. During this time, a large variety of orbital inclinations has been realized. Much of Cassini's time has been spent within the magnetosphere of Saturn. This is the cavity in the flow of the solar wind within which the effects of the magnetic field of the planet dominate over the effects of the solar wind magnetic field. In this way, it has been possible to investigate magnetic field configurations in situ both above and below the equatorial plane.

Energy flow within Saturn's magnetosphere is not completely understood. At Earth, the main source of energy is the solar wind. Interaction between the Earth's magnetosphere and the solar wind, primarily through dayside reconnection, drives the dynamics within the cavity (Dungey, 1961). By contrast, at Saturn (as at Jupiter), it is thought that the main source of energy is the comparatively much faster rotation of the planet itself (e.g., Cowley et al., 2004; Vasyliunas, 1983), as well as significant mass loading from sources within the magnetosphere. The relative contribution of internal and external drivers of magnetospheric dynamics at Saturn is an ongoing area of study (e.g., Thomsen, 2013, and references therein). Understanding the dynamics of the magnetic field configuration would lead to a greater understanding in this area.

In a perfect (plasma-free) system, the field lines of a planetary dipole would corotate exactly with the planet, in a meridional sense. However, the magnetosphere of Saturn is not a massless system, containing matter that is primarily released by the cryovolcanic moon Enceladus (Dougherty et al., 2006), among other sources. This matter is predominantly neutral, but subsequent ionization leads to a plasma source on the order of 12–3,000 kg/s (Hansen et al., 2006; Johnson et al., 2006). This results in mass loading in the equatorial regions of the magnetosphere, which acts to stretch the field lines (Hill et al., 1981). This effect is only seen within giant planet magnetospheres, since the mass loading of smaller systems (which tend to lack sources such as active moons) is too low to be significant. As a result, more angular momentum must be transferred from the planet to maintain corotation (Vasyliunas, 1983). This process is ultimately limited by the finite conductivity of the ionosphere, leading to a lag in the corotational velocity of the plasma torus. Field lines frozen to the torus subsequently exhibit a bend back with respect to the meridian planes. This phenomenon is well observed and documented both at Saturn and at Jupiter (wherein the torus is formed by the volcanic moon Io) (Wang et al., 2001). A schematic representation

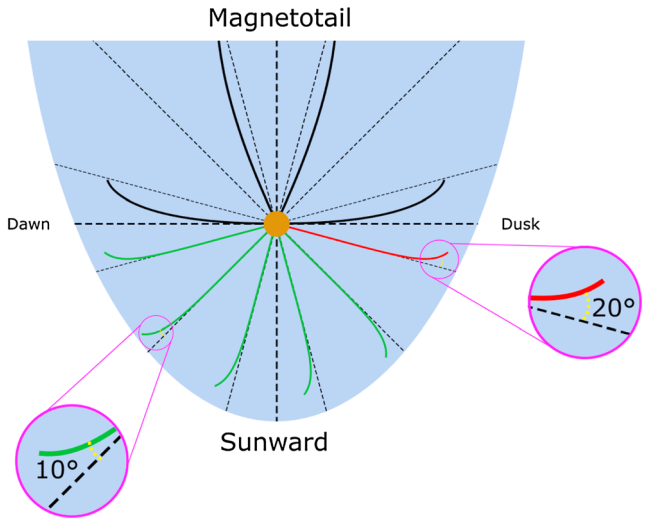

Figure 1. Cartoon illustrating Saturn's magnetosphere showing the field configuration of interest. Saturn is centered and being viewed from above the north pole. The green field lines correspond with swept back and the red with swept-forward flux tubes. The black field lines correspond with field lines being stretched into the magnetotail. Field lines return to Saturn's south pole.

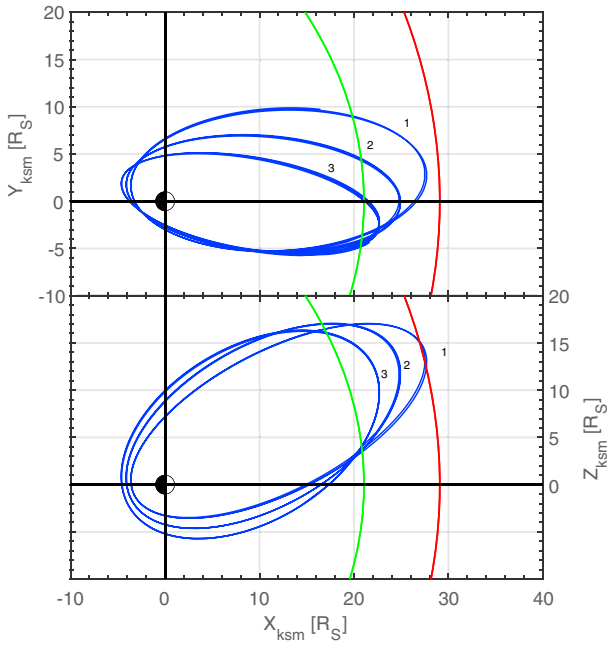

Figure 2. Trajectory plots of the orbits used in this study. Each thick blue line corresponds with a group of three orbits that lie spatially proximal to each other. The spacecraft moves in an anticlockwise sense. The labels 1, 2, and 3 correspond to the orbital groups to which reference is made in Table 1. The coordinate system used is Saturn solar magnetic (KSM). The system is centered on Saturn, with *X* pointing toward the Sun, *Y* is perpendicular to the rotation axis and points toward dusk, and *Z* is chosen such that the rotation axis lies in the *X*-*Z* plane. (top) Looks down on the planet's north pole. (bottom) The view to the dawn meridian. The green line gives the modeled magnetopause position (according to Kanani et al., 2010) and the red line the bow shock position according to Went et al. (2011).

of the configuration is shown in green in Figure 1. Here the observer looks down on a cartoon of Saturn's north pole, with bent forward field shown in red and bent back shown in green. All field lines close in the southern hemisphere. The black field lines on the nightside of the planet, some of which form the magnetotail, are not investigated in this study.

The focus of this study is the opposite configuration of the field; that is, when flux tubes are swept forward with respect to the direction of rotation. This configuration has been observed in the predusk region at Saturn (e.g., Delamere et al., 2015) and is expected to arise as a result of confinement of the planetary dipole by the magnetopause. The most significant contribution to the azimuthal field (other than the previously mentioned mass loading) is the magnetopause tail current system, which acts to twist meridionally aligned field lines toward the tail (e.g., Alexeev et al., 2006; Belenkaya et al., 2008). At dawn this results in swept back field, but at dusk it results in field lines being swept forward. This work concerns the dynamics of the configuration, using Cassini observations. Modeling of the phenomenon has previously been explored by Bunce et al. (2003) and Arridge et al. (2006).

Examples of field lines being twisted out of the meridian planes in the direction of planetary rotation were first observed at Jupiter by the Ulysses spacecraft in 1992 (Balogh et al., 1992; Dougherty et al., 1993). These observations were limited due to the nature of the Ulysses flyby at Jupiter, which was restricted to a swing-by designed to increase the inclination of the spacecraft with respect to the plane of the ecliptic. They were followed 6 years later by observations made by the spacecraft Galileo. This mission aimed specifically to investigate Jupiter's magnetosphere and involved multiple orbits, resulting in observations that were more extensive. Kivelson et al. (2002) notes a pronounced sweep-forward effect that becomes increasingly evident toward the dusk meridian. In addition, she notes an enhancement of the effect with increasing magnetic latitude.

Unfortunately, the Galileo mission also suffered from limitations with respect to these observations. The Galileo orbits where confined to equatorial plane, which rendered investigations of the high latitudes impossible. However, the wobble of Jupiter's magnetic equator with respect to its rotational equator (which occurs as a result of the offset of the two axes) allowed the spacecraft to measure latitudes that were effectively above and below the equator (Kivelson et al., 1992).

The Cassini mission is subject to no such limitations. The nature and length of the mission have resulted in a very large number of widely varying orbits, many of which are highly inclined and thus appropriate to these observations (Dougherty et al., 2004). For this work, orbits were chosen that lay very close to each other spatially, to enable temporal effects to be resolved to some extent from spatial effects. A series of orbits from early 2008 (Revs 57 through 65) fit this criterion and place the spacecraft in the appropriate latitudes in the predusk sector. In this study, this series of orbits is examined for evidence of swept-forward field, with a view to investigating the dynamics of the phenomenon.

2. Observations

The orbits studied are illustrated in Figure 2. The coordinate system used is the Kronocentric Solar Magnetospheric system. X points from Saturn to

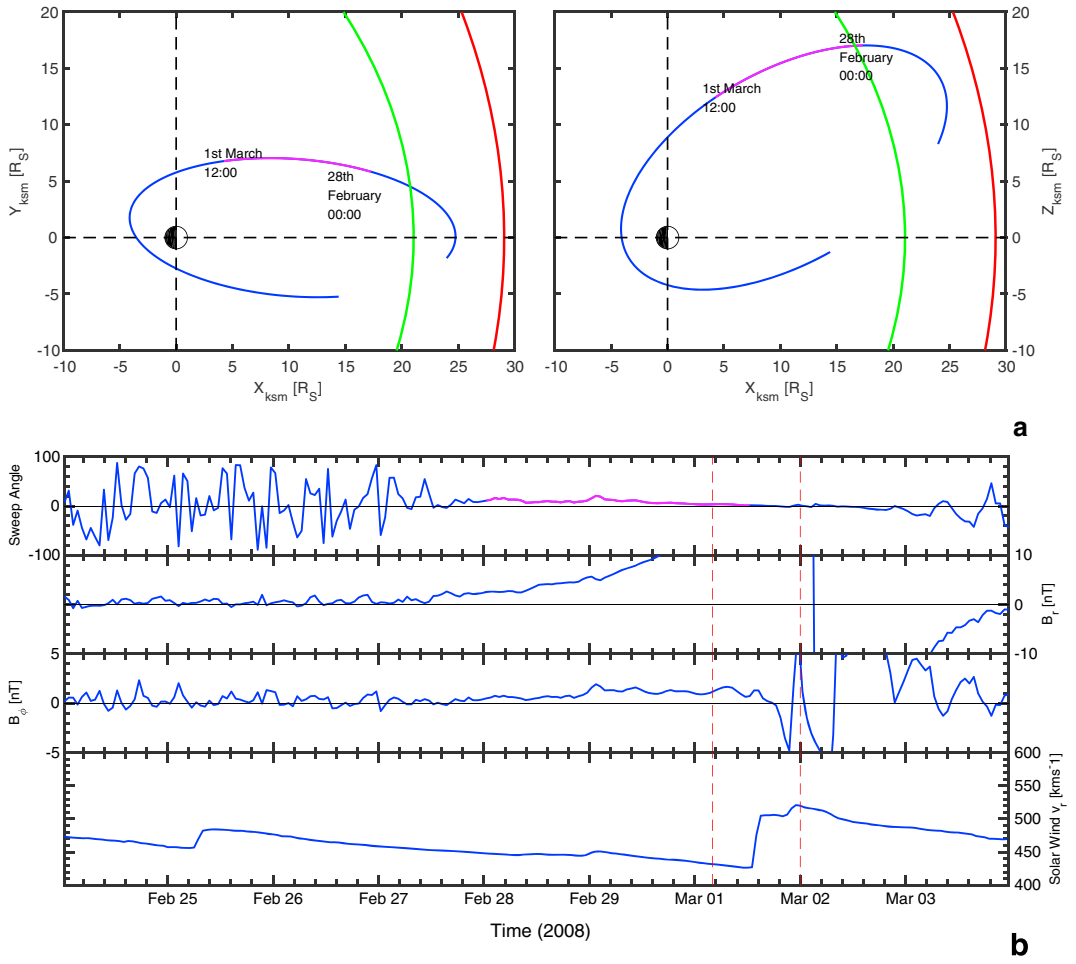

Figure 3. (a) An orbit demonstrating no particular perturbation. (b, first panel) The angle in degrees of the field with the meridian plane. (b, second and third panels) The field data for the orbit in question, from which the first panel is obtained. The coordinate system used for the field is Saturn Spherical Polar (KRTP), with the *r* component pointing away from the planet and the ϕ component pointing azimuthally in the direction of rotation. (b, fourth panel) The solar wind radial velocity, as predicted by mSWiM. The dotted red lines show the low and upper limits, respectively, on the arrival of the rapid change on 1 March. It should be noted that this shock arrives while the spacecraft is almost on the nightside of the planet and so is not expected to produce a perturbation in sweep angle. Also shown in Figure 3a are trajectory plots for orbit 2A. The coordinate system used is KSM, with the colors corresponding to regions of the first panel in Figure 3b.

the Sun, *Y* is perpendicular to the axis of rotation and points in the direction of dusk, and *Z* is chosen such that the axis of rotation lies in the *X*-*Z* plane.

Kivelson et al. (2002) defines the sweep-forward angle α (depicted in Figure 1 and given in equation (1)) as the inverse tangent of the ratio of the azimuthal component of the field to its radial component, with respect to the planet's rotation (note that Saturn's dipole axis deviates by less than 1° from its axis of rotation (e.g., Connerney et al., 1982; Giampieri & Dougherty, 2004; Smith et al., 1980).

$$\alpha = \tan^{-1}\frac{B_\phi}{B_r} \tag{1}$$

The same definition is used in this work.

All of the orbits surveyed were found to exhibit swept-forward field in the predusk region. In each case, the degree of sweep was measured and compared with the predicted solar wind velocity in the same period. The average peak (highest recorded value per orbit) angle was found to be 23° forward with respect to rotation. In total, nine orbits were surveyed, fitting into the three groups identified in Figure 2. Included in Figure 2 (as well as Figures 3 and 4) are modeled magnetopause and bow shock locations (Arridge et al., 2006; Kanani

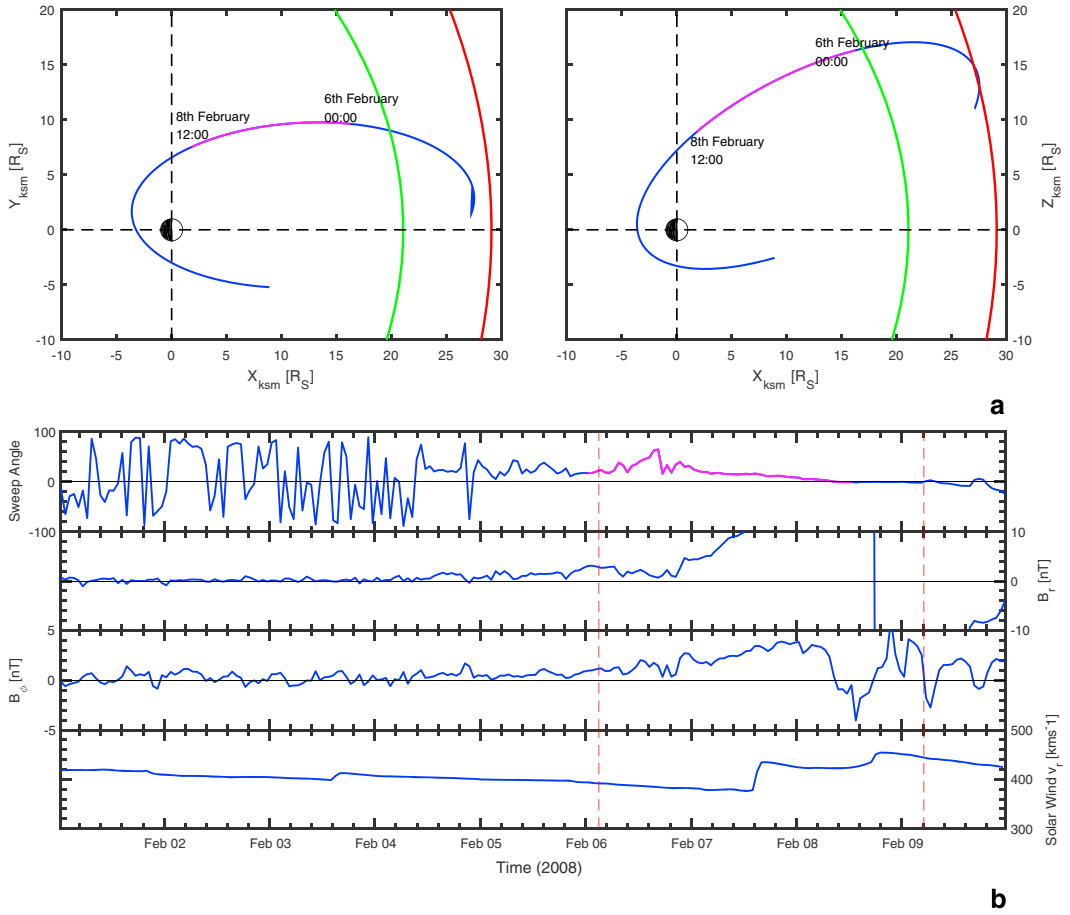

Figure 4. (a) An orbit demonstrating a perturbation corresponding with a solar wind shock arrival. (b, first panel) The angle in degrees of the field with the meridian plane. (b, second and third panels) The field data for the orbit in question, from which the first panel is obtained. The coordinate system used for the field is Saturn Spherical Polar (KRTP), with the r component pointing away from the planet and the ϕ component pointing azimuthally in the direction of rotation. (b, fourth panel) The solar wind radial velocity, as predicted by mSWiM. The dotted red lines show the lower and upper limits on the arrival of the rapid change on 7 February. Also shown in Figure 4a are trajectory plots for orbit 1B. The coordinate system used is KSM, with the colors corresponding to regions of the first panel in Figure 4b.

et al., 2010; Went et al., 2011) for typical solar wind conditions, with a solar wind dynamic pressure of 0.028 nPa. Within each group, the orbits lie almost on top of each other, with a maximum deviation of 0.2 R_s. The groups are separated by a distance of approximately 1 R_s in the region of interest, suggesting that cross-group comparison is still useful in resolving temporal effects. Each orbit took a little over 1 week to complete, which is the limiting factor in the timescale of the monitoring. The sweep angle was determined using measurements of the field from the MAG instrument (Dougherty et al., 2004). An example of one of the surveyed orbits is shown in Figure 3, together with its associated trajectory. The trajectory is plotted in Figure 3a and involves part of Rev 60. The radial and azimuthal components of the total magnetic field are plotted in Figure 3b (second and third panels, respectively) with the sweep angle derived from these components plotted in the first panel. The fourth panel shows solar wind radial velocity as modeled by the Michigan Solar Wind Model (see section 3).

The first section (shown in blue) of the orbit is located within the equatorial region and includes a possible magnetopause crossing. The measurement of sweep angle is therefore likely dominated by external fields or effects not taken into account in this study. The second section (shown in pink) shows a consistently swept-forward field, the degree of which drops off as the spacecraft descends toward the nightside equator. This corresponds with the radial component of the field becoming extremely large as the spacecraft enters the postdusk, premidnight sector. The sweep angle also drops off as the spacecraft descends toward the

Table 1
A Summary of the Orbits Surveyed

Event start date	Event end date	Orbit	Maximum forward angle	Time from AO	Shock present	Shock time	Max. shock error
25 Jan	27 Jan	1A (Rev 57)	29.60	−59	No		20
6 Feb	8 Feb	1B (Rev 58)	64.78	−47	Yes	+24	37
18 Feb	20 Feb	1C (Rev 59)	47.12	−35	No		30
28 Feb	1 Mar	2A (Rev 60)	20.57	−25	No		10
10 Mar	12 Mar	2B (Rev 61)	41.21	−14	Yes	−25	20
20 Mar	23 Mar	2C (Rev 62)	25.85	−4	No		10
30 Mar	1 Apr	3A (Rev 63)	22.20	+6	No		10
9 Apr	11 Apr	3B (Rev 64)	24.67	+16	Yes	−15	20
18 Apr	19 Apr	3C (Rev 65)	16.43	+25	No		17

Note. Maximum forward angle is measured in degrees. Time from apparent opposition is measured in days, and shock time is measured in hours. The sign on the shock time indicates whether it was predicted to have arrived before the peak in sweep angle (negative) or after (positive). The maximum shock time error column presents the largest recorded time discrepancy (in hours) between the prediction of a shock arrival and its measurement by spacecraft as presented in the work by Zieger and Hansen (2008). The windows in shock arrival times shown in Figures 3 and 4 are based upon this column.

equator, where the radial and azimuthal fields change direction, which renders the measurement of a sweep angle meaningless.

The orbit shown in Figure 3 corresponds to a predicted quiescent period in the solar wind, where the peak sweep angle is 21° (recorded on 29 February at 01:30). This value is close to the average value recorded during quiescent periods (23°). Quiescent periods were defined as orbits that did not include an hourly variation in sweep angle of more than the magnitude of the lowest value recorded during the orbit between 16:00 and 18:00 LT. For example, for the orbit depicted in Figure 3, this value is 3°, and in no hour during which the spacecraft was between 16:00 and 18:00 LT did the degree of sweep vary by more than 3°. Figure 3 shows a representative example of such an orbit, with a consistent sweep-forward angle existing in the region of interest, but no major perturbations occurring. The data are taken from the 1 h time resolution magnetometer data series.

In contrast, Figure 4 shows the angle measurements for an orbit demonstrating a transient event. The trajectory is plotted in Figure 4a and involves part of Rev 58. Once again, the radial and azimuthal components of the total magnetic field are plotted in Figure 4b (second and third panels, respectively) with the sweep angle derived from these components plotted in the first panel. The fourth panel shows solar wind radial velocity as modeled by the Michigan Solar Wind Model (mSWiM) (see section 3). A large perturbation is clearly present in sweep angle on 6 February at 16:30, which disturbs an otherwise typical orbital profile. It corresponds to a change in the azimuthal component of the field. A maximum angle of 64.78° is recorded, more than triple the background value of 19°. This represents the largest sweep angle recorded in this study. The perturbation remains to a lesser extent in the subsequent orbit, before the field relaxes again to its quiescent state. This behavior seems to be consistent throughout the orbits surveyed, with the field being periodically perturbed and then relaxing (although to a much lesser degree in the group 3 orbits). This is summarized in Table 1. The table shows an overview of each orbit used in this study, including the start and end times of the events recorded, to which Rev the orbit belongs; the maximum sweep angle recorded (positive in the positive azimuthal direction); and details regarding the mSWiM propagations (see section 3). Group 3 seems to include a period of relaxation, although a significant perturbation is not recorded. It is possible that a perturbation occurred prior to the arrival of Cassini in the region of interest. It is also possible that the lower values of sweep angle are a result of the difference in spacecraft position that corresponds with each group. As the orbits progress from group 1 to group 3, the spacecraft moves on average closer to Saturn, with the 1B peak occurring at a distance of 24.1 R_S, the 2B peak at 22.6 R_S, and the 3B peak at 20.1 R_S. It is likely that any solar wind-based influence on the field configuration would lessen closer to the planet. Another possibility is that the group 3 orbits correspond with a period of solar wind rarefaction.

3. Discussion

The perturbations recorded could be a result of internal or external factors. Delamere et al. (2015) notes the possibility of reconnection in the magnetodisk resulting in internal momentum transfer within Saturn's

magnetosphere, leading to swept-forward field. Such effects are not considered in this study and may be the topic of future work. Another internal factor affecting the azimuthal configuration of the field is the planetary period oscillation (PPO) system. External driving meanwhile is likely to involve the effects of solar wind interaction with Saturn's magnetosphere.

A ubiquitous feature throughout the magnetosphere of Saturn is the modulation close to the planetary rotation period of magnetic fields, plasma populations and waves, and radio emissions (e.g., Cowley et al., 2006; Provan et al., 2016; Southwood & Kivelson, 2007). Studies (such as those referenced above) have shown that two systems are present, one associated with the northern hemisphere and one associated with the southern hemisphere. Distinguishing the influence of these systems on phenomena becomes easier during times wherein their modulation periods are most separate. Fortunately for this work, early 2008 represents such a time (see, for example, Provan et al., 2015, Figure 2), with the northern and southern periods being separated by approximately 0.2 h.

A detailed analysis of the effects of the PPO on the northern azimuthal field configuration in the early part of 2008 was previously performed by Hunt et al. (2015), following their study on the southern configuration (Hunt et al., 2014). They suggested that a phase asymmetry due to latitudinal motion of northern system currents to lower latitudes at a northern phase of 90° would result in the positive half cycle oscillations in B_ϕ being larger in amplitude than the negative half cycle oscillations. These perturbations form a weakly leading field configuration. As such, the largest effect of the PPO would be seen at a northern phase of 90° and a southern phase of 270°. It seems highly likely therefore that the effect of the PPO could contribute to the establishment of the background swept-forward configuration noted in this work. This is consistent with the determined magnitude of the B_ϕ perturbation (see Figure 11 from Hunt et al., 2015) which is on the order of 5 nT as are the perturbations recorded in this work. It does not seem likely that the PPO could be entirely responsible for the observed highly perturbed field configurations in orbits 1B and 2B (Revs 58 and 61) as the recorded peaks do not correspond entirely with these phases of the northern and southern PPO systems. The peak in orbit 1B occurs at a northern phase Ψ_N of 179 ± 33° and the peak in 2B at Ψ_N = 12 ± 35° where the error represents an hour either side of the recorded peak position. Only the northern phases was examined given the position of the events recorded in this study and the fact that 2008 represents a period of clear northern/southern phase separation (see Provan et al., 2016, Figure 11). In addition, the recorded peaks occur equatorward of the largest perturbations in B_ϕ discussed by Hunt et al. (2015) (see Figure 3 of that work), although it should be noted that parts of orbits 1C and onward (Revs 58–65) are analyzed within that study.

In order to investigate the influence of the solar wind with regard to the recorded perturbations, results from the Michigan Solar Wind Model (mSWiM) were employed. This decision was made based on the comprehensive validation of this model, carried out against spacecraft data (Zieger & Hansen, 2008). The model is a 1.5-D ideal MHD simulation that outputs solar wind variables as a function of heliocentric distance and time. It propagates solar wind conditions at 1 AU, as measured by a variety of spacecraft positioned at Earth-Sun L1, radially outward along an inertial line defined by the time of Sun-Earth-target alignment in heliocentric longitude. The model output is extracted at the heliocentric distance of the target body, here Saturn, at each time step. Because both the Earth and Saturn move in their orbits relative to the inertial line, the relative orbital motion is taken into account by rotating both the input conditions (at Earth) and the output values (at the target) to the inertial line. For this reason, the propagation is most effective at the time when rotations are minimized. This optimally occurs when plasma leaving the Earth at the time of alignment (opposition: Sun-Earth-Target) reaches the target. This time is called the apparent opposition by Zieger and Hansen (2008).

The field displays an inherent sweep forward in the region surveyed, consistent with a dipolar field confined by a magnetopause layer. However, when subject to a sudden velocity increase of the solar wind, the degree of sweep increases significantly, followed by a period of relaxation of the field. This is shown in Figure 4 (bottom). Note that not every set of measurements supports this; group 3 orbits in particular demonstrate no particular increase in the degree of sweep when subjected to the predicted shock. This could be explained by inaccuracies in mSWiM (group 3 orbits taking place further from apparent opposition than group 2) or by other magnetospheric factors (such as internal reconnection or other transitory events) that have not been considered here but act to constrain the field to the meridional planes.

The uncertainty in the mSWiM values has been quoted and is detailed by Zieger and Hansen (2008). The significant uncertainty for this study lies in the shock arrival time, since the suggestions made rely on shocks

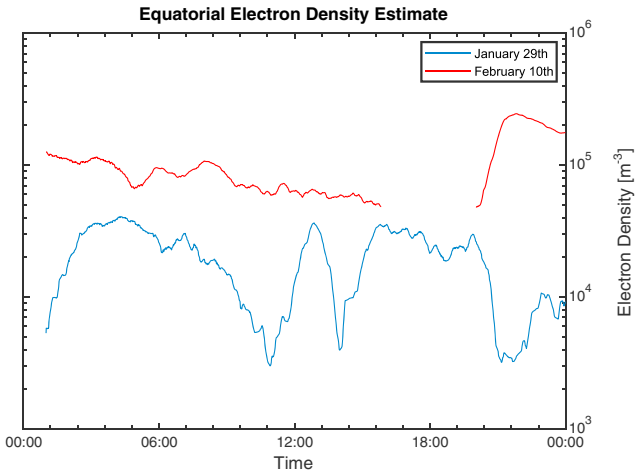

Figure 5. Electron density moments taken using the CAPS instrument. A single direction is examined and spatial isotropy assumed. The readings shown here were taken when the spacecraft passed through the dayside equatorial plane prior to orbit 1B (blue) and subsequently when it returned to this position following orbit 1B (red). An increase in the order of magnitude of the electron density measured suggests a possible compression of the magnetosphere, which could result from a solar wind shock.

arriving at Saturn prior to the measurements of peak sweep-forward angles. For a shock to be considered for the purposes of this work, particularly with reference to Table 1, the window of its arrival must correspond to the measurement of the peak sweep-forward angle. The referenced work expands in detail upon the capabilities of the model. In general, solar wind velocity is the most reliable output of the model. The model is most reliable during periods of low solar activity corresponding with apparent opposition.

Periods of low solar activity, which tend to occur in the late declining or early ascending phases of the solar cycle, correspond to quiescent periods in the solar wind. These periods reflect slower dynamic changes on the surface of the Sun, as well as fewer transient events such as coronal mass ejections. As a result, the conditions of the solar wind may be predicted during these periods with relatively high accuracy. The reliability of the results of the model is quantified in a correlation coefficient, the result of significant statistical analysis and validation.

Fortunately for the purposes of this study, the orbits used both roughly coincide with solar minimum and take place close to apparent opposition between Earth and Saturn. In addition, the only output required from the model is the solar wind velocity, in order to locate solar wind shocks. These events correspond with a change in dynamic pressure, representing an external driver of magnetospheric dynamics (e.g., Crary et al., 2005, and references therein).

Another possible variable to consider when checking for possible shock events is the plasma mass density of the magnetosphere at the time. It is reasonable to assume that a compression of the magnetosphere would lead to a perturbation in the local mass density. Unfortunately, the plasma environment local to the spacecraft in the latitudes at which swept-forward field is measured is extremely tenuous. As such, measurements of local plasma density are unavailable. Instead, an estimate for the equatorial electron number density was made before and after shocks were predicted to have arrived, in the same equatorial spatial position, in order to investigate this possibility at least on a qualitative basis. To arrive at this estimate, the equatorial electron number density is taken as a proxy for the total mass contained within the dayside plasma sheet. These measurements were taken by anode 5 (of eight similar anodes) of the Cassini Plasma Spectrometer (CAPS) instrument (Young et al., 2004), which detects electrons within a 20° field of view and assumes isotropy in order to derive electron number densities (Lewis et al., 2010). The time resolution for the energy spectra is 2 s.

The measurements were taken as the spacecraft headed up out of the equatorial plane, approaching noon local time. In general, a predicted shock corresponds with an increase of electron density in the dayside magnetosphere, supporting the occurrence of a subsequent magnetosphere compression. Such an increase is illustrated in Figure 5, corresponding with the shock predicted to occur by mSWiM on 7 February 2008 (shown in Figure 4). Figure 5 also shows a pronounced increase in number density, following the data gap on 10 February 2008. It is thought that this corresponds to Cassini being in the magnetosheath, lending credence to the suggestion of magnetospheric compression.

In general, confinement of the planetary dipolar field gives rise to predusk swept-forward field configurations. The measured average angle during quiescent periods (23°) is representative of this expected structure (see Arridge et al., 2006; Bunce et al., 2003). Perturbations of this configuration could result from magnetospheric compression, for example, as a result of solar wind shocks, or by some other interaction with the solar wind. The mechanisms by which momentum is transferred from the solar wind to the magnetospheric plasma are as yet unclear, and the subject of future work. In this work, three possibilities are considered. In either of the first two cases, it is the response of the system following a compression resulting from a shock in the solar wind that is considered.

It is possible that conservation of angular momentum within the magnetospheric system could explain a period of super corotation of magnetodisk plasma following a compression. A rotating system must rotate faster when compressed in order for angular momentum to be conserved. Equatorial plasma accelerated in such a way would drag the frozen in field lines with it, leading to a field configuration matching the swept-forward

profile. This proposition assumes that the system is torque free. The extent to which Saturn's magnetosphere can be considered torque free is not precisely clear. There are certainly torques present in the system but the timescales over which they act vary. In general, the Alfvén speed is a good guideline for the torque transmission. If the timescale over which the compression of the system occurs is significantly shorter than the time, it would take an Alfvén wave to propagate from the planet (the source of rotation) to the boundary, then there is a good basis to consider the event torque free. In this case, it would be reasonable to expect an acceleration in the flow of the dayside plasma sheet, which would have the effect of dragging field lines forward. This would be a global effect, which would manifest in sectors other than predusk. It can therefore not be entirely responsible for the configuration of the system during a transitory event but could be a contributing factor. Measurements of the plasma flow would be helpful in determining how big a contribution this effect could have; unfortunately, such measurements are impossible to take concurrent to the field line measurements given the spacecraft's position. Local plasma measurements are not useful, given the highly tenuous nature of the plasma at the latitudes of the field measurements.

The effects of magnetosphere currents are also considered. Kivelson et al. (2002) notes that (at Jupiter) flux tubes crossing the equatorial current sheet near the magnetopause would be twisted tailward by magnetopause currents. This would give rise to a quiescent swept-forward configuration. In addition, a compression of the boundary layer would result in a local increase of current density, strengthening the corotation enforcement current (CEC) (Moriguchi et al., 2008). This would act to bring the field lines closer in line with the meridian planes but could not lead to a swept-forward configuration directly. This interaction would be expected to take place at the equator, since the CECs are field-aligned, and thus force-free at higher latitudes.

Finally, it is important to consider the effects of direct momentum transfer from the solar wind. Mass transport from the magnetosheath into the magnetosphere can occur across the boundary layer, for example, by means of the Kelvin-Helmholtz instability (Nykyri & Otto, 2001). In this way, fast flowing (in the direction of rotation at dusk) matter from the solar wind could enter the magnetosphere and either accelerate the local plasma flow or become itself frozen to the field lines and drag them forward directly. Such an occurrence would have greatest effect at the dawn-dusk plane, where the bulk flow velocity is perpendicular to the plane of the meridian. At the dawn side, the effect would be to drag the field back, whereas at dusk, the converse would be true. This effect could give rise to both the quiescent and transitory configurations, depending on the velocity profile of the solar wind.

In order to support the prediction of shock arrivals, radio and plasma data sets were examined. Radio signatures in the Radio Plasma and Waves Science (Gurnett et al., 2004) instrument data are sometimes present when the magnetosphere of Saturn experiences compression due to solar wind shocks. Such signatures are often characterized by a long-term extension into the 10^4 kHz range corresponding to SKR bursts (Badman et al., 2008). This examination was inconclusive. It is important to note that while the presence of such signatures lends credence to the assumption of a solar wind shock, it does not confirm such an occurrence. Similarly, the lack of such signatures does not preclude a shock since there are many other factors affecting SKR bursts.

4. Concluding Remarks

This work has presented a series of Cassini orbits from 2008 that correspond with high-latitude observations of the region surrounding the dusk terminator. The field in the region was examined and found to exhibit a swept-forward configuration. The temporal behavior of this configuration was examined, based on the spatial coherence of the orbits used. It was suggested, based on work carried out by Hunt et al. (2015), that the modulation of the azimuthal component of the magnetic field by the planetary period oscillation is at least partially responsible for the background "quiescent" swept-forward configuration. A pattern of perturbation and relaxation was established, and found in two cases to correspond which the arrival of solar wind shocks, as predicted by mSWiM. Mechanisms by which these shocks could lead to a swept-forward configuration were outlined. Future work will focus on a comprehensive mapping of the field configuration in space, as well as a more detailed investigation into the mechanisms of solar wind momentum transfer. This survey will begin with dawnside mapping to establish the effect of solar wind processes, as well as the influence of the PPOs, on this side of the planet.

Acknowledgments
We thank Cassini instrument Principal Investigators D.T. Young, and J.H. Waite. This work was supported by UK STFC through consolidated grants to MSSL/UCL and Imperial College London. E.D. is supported by an STFC PhD studentship. A.M. is supported by a Royal Society University Research Fellowship. All MAG data used in this study are available at NASA PDS: https://pds-ppi.igpp.ucla.edu/. All mSWiM data are available at http://mswim.engin.umich.edu/

References

Alexeev, I. I., Kalegaev, V. V., Belenkaya, E. S., Bobrovnikov, S. Y., Bunce, E. J., Cowley, S. W. H., & Nichols, J. D. (2006). A global magnetic model of Saturn's magnetosphere and a comparison with Cassini SOI data. *Geophysical Research Letters*, *33*, L08101. https://doi.org/10.1029/2006GL025896

Arridge, C. S., Achilleos, N., Dougherty, M. K., Khurana, K. K., & Russell, C. T. (2006). Modeling the size and shape of Saturn's magnetopause with variable dynamic pressure. *Journal of Geophysical Research*, *111*, A11227. https://doi.org/10.1029/2005JA011574

Badman, S. V., Cowley, S. W. H., Lamy, L., Cecconi, B., & Zarka, P. (2008). Relationship between solar wind corotating interaction regions and the phasing and intensity of Saturn kilometric radiation bursts. *Annales de Geophysique*, *26*(12), 3641–3651. https://doi.org/10.5194/angeo-26-3641-2008

Balogh, A., Dougherty, M. K., Forsyth, R. J., Southwood, D. J., Smith, E. J., Tsurutani, B. T., … Burton, M. E. (1992). Magnetic field observations during the Ulysses flyby of Jupiter. *Science*, *257*(5076), 1515–1518. https://doi.org/10.1126/science.257.5076.1515

Belenkaya, E. S., Cowley, S. W. H., Badman, S. V., Blokhina, M. S., & Kalegaev, V. V. (2008). Dependence of the open-closed field line boundary in Saturn's ionosphere on both the IMF and solar wind dynamic pressure: Comparison with the UV auroral oval observed by the HST. *Annales de Geophysique*, *26*(1), 159–166. https://doi.org/10.5194/angeo-26-159-2008

Bunce, E. J., Cowley, S. W. H., & Wild, J. A. (2003). Azimuthal magnetic fields in Saturn's magnetosphere: Effects associated with plasma sub-corotation and the magnetopause-tail current system. *Annales de Geophysique*, *21*(8), 1709–1722. https://doi.org/10.5194/angeo-21-1709-2003

Connerney, J. E. P., Ness, N. F., & Acuna, M. H. (1982). Zonal harmonic model of Saturn's magnetic field from Voyager 1 and 2 observations. *Nature*, *298*(5869), 44–46. https://doi.org/10.1038/298044a0

Cowley, S. W. H., Bunce, E. J., & O'Rourke, J. M. (2004). A simple quantitative model of plasma flows and currents in Saturn's polar ionosphere. *Journal of Geophysical Research*, *109*, A05212. https://doi.org/10.1029/2003JA010375

Cowley, S. W. H., Wright, D. M., Bunce, E. J., Carter, A. C., Dougherty, M. K., Giampieri, G., … Robinson, T. R. (2006). Cassini observations of planetary-period magnetic field oscillations in Saturn's magnetosphere: Doppler shifts and phase motion. *Geophysical Research Letters*, *33*, L07104. https://doi.org/10.1029/2005GL025522

Crary, F. J., Clarke, J. T., Dougherty, M. K., Hanlon, P. G., Hansen, K. C., Steinberg, J. T., … Young, D. T. (2005). Solar wind dynamic pressure and electric field as the main factors controlling Saturn's aurorae. *Nature*, *433*(7027), 720–722. https://doi.org/10.1038/nature03333

Delamere, P. A., Otto, A., Ma, X., Bagenal, F., & Wilson, R. J. (2015). Magnetic flux circulation in the rotationally driven giant magnetospheres. *Journal of Geophysical Research: Space Physics*, *120*, 4229–4245. https://doi.org/10.1002/2015JA021036

Dougherty, M. K., Southwood, D. J., Balogh, A., & Smith, E. J. (1993). Field-aligned currents in the Jovian magnetosphere during the Ulysses flyby. *Planetary and Space Science*, *41*(4), 291–300. https://doi.org/10.1016/0032-0633(93)90024-v

Dougherty, M. K., Kellock, S., Southwood, D. J., Balogh, A., Smith, E. J., Tsurutani, B. T., … Cowley, S. W. H. (2004). The Cassini magnetic field investigation. *Space Science Reviews*, *114*(1-4), 331–383. https://doi.org/10.1007/s11214-004-1432-2

Dougherty, M. K., Khurana, K. K., Neubauer, F. M., Russell, C. T., Saur, J., Leisner, J. S., & Burton, M. E. (2006). Identification of a dynamic atmosphere at Enceladus with the Cassini magnetometer. *Science*, *311*(5766), 1406–1409. https://doi.org/10.1126/science.1120985

Dungey, J. W. (1961). Interplanetary magnetic field and the auroral zones. *Physical Review Letters*, *6*(2), 47–48. https://doi.org/10.1103/PhysRevLett.6.47

Giampieri, G., & Dougherty, M. K. (2004). Rotation rate of Saturn's interior from magnetic field observations. *Geophysical Research Letters*, *31*, L16701. https://doi.org/10.1029/2004GL020194

Gurnett, D. A., Kurth, W. S., Kirchner, D. L., Hospodarsky, G. B., Averkamp, T. F., Zarka, P., … Pedersen, A. (2004). The Cassini radio and plasma wave investigation. *Space Science Reviews*, *114*(1-4), 395–463. https://doi.org/10.1007/s11214-004-1434-0

Hansen, C. J., Esposito, L., Stewart, A. I. F., Colwell, J., Hendrix, A., Pryor, W., … West, R. (2006). Enceladus' water vapor plume. *Science*, *311*(5766), 1422–1425. https://doi.org/10.1126/science.1121254

Hill, T. W., Dessler, A. J., & Maher, L. J. (1981). Corotating magnetospheric convection. *Journal of Geophysical Research*, *86*(A11), 9020–9028. https://doi.org/10.1029/JA086iA11p09020

Hunt, G. J., Cowley, S. W. H., Provan, G., Bunce, E. J., Alexeev, I. I., Belenkaya, E. S., … Coates, A. J. (2014). Field-aligned currents in Saturn's southern nightside magnetosphere: Subcorotation and planetary period oscillation components. *Journal of Geophysical Research: Space Physics*, *119*, 9847–9899. https://doi.org/10.1002/2014JA020506

Hunt, G. J., Cowley, S. W. H., Provan, G., Bunce, E. J., Alexeev, I. I., Belenkaya, E. S., … Coates, A. J. (2015). Field-aligned currents in Saturn's northern nightside magnetosphere: Evidence for interhemispheric current flow associated with planetary period oscillations. *Journal of Geophysical Research: Space Physics*, *120*, 7552–7584. https://doi.org/10.1002/2015JA021454

Johnson, R. E., Smith, H. T., Tucker, O. J., Liu, M., Burger, M. H., Sittler, E. C., & Tokar, R. L. (2006). The Enceladus and OH Tori at Saturn. *The Astrophysical Journal Letters*, *644*(2), L137–L139. https://doi.org/10.1086/505750

Kanani, S. J., Arridge, C. S., Jones, G. H., Fazakerley, A. N., McAndrews, H. J., Sergis, N., … Krupp, N. (2010). A new form of Saturn's magnetopause using a dynamic pressure balance model, based on in situ, multi-instrument Cassini measurements. *Journal of Geophysical Research*, *115*, A06207. https://doi.org/10.1029/2009JA014262

Kivelson, M. G., Khurana, K. K., Means, J. D., Russell, C. T., & Snare, R. C. (1992). The Galileo magnetic-field investigation. *Space Science Reviews*, *60*(1–4), 357–383. https://doi.org/10.1007/bf00216862

Kivelson, M. G., Khurana, K. K., & Walker, R. J. (2002). Sheared magnetic field structure in Jupiter's dusk magnetosphere: Implications for return currents. *Journal of Geophysical Research*, *107*(A7), 107. https://doi.org/10.1029/2001JA000251

Lewis, G. R., Arridge, C. S., Linder, D. R., Gilbert, L. K., Kataria, D. O., Coates, A. J., … Livi, S. A. (2010). The calibration of the Cassini-Huygens CAPS electron spectrometer. *Planetary and Space Science*, *58*(3), 427–436. https://doi.org/10.1016/j.pss.2009.11.008

Moriguchi, T., Nakamizo, A., Tanaka, T., Obara, T., & Shimazu, H. (2008). Current systems in the Jovian magnetosphere. *Journal of Geophysical Research*, *113*, A05204. https://doi.org/10.1029/2007JA012751

Nykyri, K., & Otto, A. (2001). Plasma transport at the magnetospheric boundary due to reconnection in Kelvin-Helmholtz vortices. *Geophysical Research Letters*, *28*(18), 3565–3568. https://doi.org/10.1029/2001GL013239

Provan, G., Tao, C., Cowley, S. W. H., Dougherty, M. K., & Coates, A. J. (2015). Planetary period oscillations in Saturn's magnetosphere: Examining the relationship between abrupt changes in behavior and solar wind-induced magnetospheric compressions and expansions. *Journal of Geophysical Research: Space Physics*, *120*, 9524–9544. https://doi.org/10.1002/2015JA021642

Provan, G., Cowley, S. W. H., Lamy, L., Bunce, E. J., Hunt, G. J., Zarka, P., & Dougherty, M. K. (2016). Planetary period oscillations in Saturn's magnetosphere: Coalescence and reversal of northern and southern periods in late northern spring. *Journal of Geophysical Research: Space Physics*, *121*, 9829–9862. https://doi.org/10.1002/2016JA023056

Smith, E. J., Davis, L., Jones, D. E., Coleman, P. J., Colburn, D. S., Dyal, P., & Sonett, C. P. (1980). Saturn's magnetosphere and its interaction with the solar wind. *Journal of Geophysical Research*, *85*(A11), 5655–5674. https://doi.org/10.1029/JA085iA11p05655

Southwood, D. J., & Kivelson, M. G. (2007). Saturnian magnetospheric dynamics: Elucidation of a camshaft model. *Journal of Geophysical Research*, *112*, A12222. https://doi.org/10.1029/2007JA012254

Thomsen, M. F. (2013). Saturn's magnetospheric dynamics. *Geophysical Research Letters*, *40*, 5337–5344. https://doi.org/10.1002/2013GL057967

Vasyliunas, V. M. (1983). Plasma distribution and flow. In A. J. Dessler (Ed.), *Physics of the Jovian magnetosphere* (pp. 395–453). Cambridge: Cambridge University Press. https://doi.org/10.1017/CBO9780511564574.013

Wang, Y., Russell, C. T., & Raeder, J. (2001). The Io mass-loading disk: Model calculations. *Journal of Geophysical Research*, *106*(A11), 26243–26260. https://doi.org/10.1029/2001JA900062

Went, D. R., Hospodarsky, G. B., Masters, A., Hansen, K. C., & Dougherty, M. K. (2011). A new semiempirical model of Saturn's bow shock based on propagated solar wind parameters. *Journal of Geophysical Research*, *116*, A07202. https://doi.org/10.1029/2010JA016349

Young, D. T., Berthelier, J. J., Blanc, M., Burch, J. L., Coates, A. J., Goldstein, R., … Zinsmeyer, C. (2004). Cassini plasma spectrometer investigation. *Space Science Reviews*, *114*(1-4), 1–112. https://doi.org/10.1007/s11214-004-1406-4

Zieger, B., & Hansen, K. C. (2008). Statistical validation of a solar wind propagation model from 1 to 10 AU. *Journal of Geophysical Research*, *113*, A08107. https://doi.org/10.1029/2008JA013046